ELSEVIER

Journal of Nuclear Materials 278 (2000) 258–265

journal of nuclear materials

www.elsevier.nl/locate/jnucmat

Displacement energy surface in 3C and 6H SiC

R. Devanathan [a], W.J. Weber [b,*]

[a] *Department of Metallurgical Engineering, Indian Institute of Technology Madras, Chennai 600036, India*
[b] *Pacific Northwest National Laboratory, MSIN K2-44, P.O. Box 999, Richland, WA 99352, USA*

Received 19 July 1999; accepted 21 September 1999

Abstract

The phase stability of 3C–SiC upon heating and the threshold displacement energy (E_d) surfaces for C and Si primary knock-on atoms (PKAs) in 3C–SiC and 6H–SiC have been investigated using molecular dynamics simulations. A recently optimized Tersoff potential is used in conjunction with an ab initio repulsive potential to represent the interactions between atoms. The simulations provide important insights into phase separation of SiC upon heating, and indicate a strong anisotropy in the E_d surface for both Si and C PKAs. The two polytypes show many similarities in the nature of the E_d surface. The average displacement energy is separately determined by simulating 30 different 500 eV cascades in 3C–SiC. The minimum displacement energies of 21 eV for C and 35 eV for Si are in excellent agreement with interpretation of experimental observations and the simulations of 500 eV cascades.

PACS: 02.70.Ns; 61.20.Ja; 61.72.Bb; 61.80.Az; 61.82.Fk

1. Introduction

Silicon carbide (SiC) composites are a leading candidate material for low-activation structural applications in proposed fusion reactors because of their excellent elevated temperature properties, radiation stability, thermal conductivity, and chemical compatibility with the fusion environment [1]. In addition, SiC is a wide band gap (~3 eV) semiconductor with a higher breakdown field, saturated electron drift velocity, and thermal conductivity than Si. This combination of properties makes SiC attractive for high-power and high-frequency electronic device applications [2]. SiC devices can also be used for direct monitoring of processes in radiation, high-temperature, and caustic environments [3]. The small diffusion coefficients of dopants preclude selective doping of SiC by diffusion [2]. The alternative is ion-implantation that introduces atomic-level defects in the material, which can lead to amorphization at high implantation doses. Such defects are also created in SiC during exposure to high-radiation environments.

A fundamental understanding of defect creation, accumulation, and recovery in SiC is needed to advance electronic device fabrication and assess the performance of components in high-radiation environments. One of the most important defect parameters that determine the extent of lattice damage is the threshold displacement energy, E_d. This is defined as the minimum kinetic energy to be transferred to an atom to displace it from its lattice site, which thereby creates a stable Frenkel pair. Several experimental studies have been performed to estimate E_d in SiC. The experiments typically involve irradiation with electrons or light ions over a range of energies to create isolated Frenkel pairs followed by an examination of defect cluster formation, amorphization, luminescence, minority carrier lifetime (MCL), resistivity changes, or relative disorder [4–8]. These experimental studies have yielded E_d values over a broad range due to uncertainty over the sublattice corresponding to the measured value of E_d and fundamental differences between experimental techniques. For instance, transmission electron microscopy (TEM) probes E_d along the

* Corresponding author. Tel.: +1-509 375 2299; fax: +1-509 375 2186.
E-mail address: bill.weber@pnl.gov (W.J. Weber).

0022-3115/00/$ - see front matter
PII: S0022-3115(99)00266-4

direction of the electron beam, while Rutherford backscattering spectroscopy/channeling (RBS/C) measurements examine average values on a specific sublattice for a given incident ion.

Silicon carbide also exhibits polytypism, which introduces a further level of complexity in analyzing published experimental data. SiC occurs in the form of more than 150 polytypes of which one (3C) is cubic and the rest are hexagonal. All SiC polytypes consist of corner-sharing CSi_4 and SiC_4 tetrahedra but differ in the stacking sequence of identical atomic planes along a principal crystallographic axis [3]. Of these, 3C–SiC and 6H–SiC have been extensively studied, because they are of the most interest for semiconductor devices. Table 1 compares the structures of 3C–SiC and 6H–SiC. The experimentally determined values of threshold displacement energy for these two polytypes are shown in Table 2. The results show considerable scatter over nearly an order of magnitude.

Based on an evaluation of literature data, Zinkle and Kinoshita [9] have recommended average E_d values of 20 and 40 eV for the C and Si sublattices, respectively, but have pointed out that further work is needed to verify the accuracy of the experimental data. In an effort to interpret the experimental data, molecular dynamics (MD) simulations have been used to examine the displacement energy surface in SiC [10–15]. MD simulations are ideally suited to the study of defect formation processes occurring over length (nm) and time (ps) scales that are too small to permit direct experimental observation. Comparison of MD results with experimental observations aids the interpretation of experimental results and helps refine the interatomic potentials used to describe the interactions between atoms in the simulation. Most of the previous simulations have used the Pearson [16] or Tersoff [17–19] potentials. The simulations have been limited to 3C–SiC and to a few low-index directions. The calculated E_d values for these directions, at or below room temperature, are shown in Table 3 for the different potentials. It is now well established that the Pearson potential is unsuitable for modeling SiC [20]. Among the studies that have used the Tersoff potential, differences arise from the choice of parameters and the nature of the short-range potential. Recently, the SiC interatomic potential has been optimized by combining the Tersoff potential, using the latest parameters, with a short-range potential derived from first-principles calculations [13,21]. Preliminary calculation of E_d along low-index directions in 3C–SiC by the present authors using the optimized potential [13] has shown excellent agreement with the results of a recent first principles calculation [15], as shown in Table 3.

The present work extends our study of threshold displacement energies to 26 directions in 3C–SiC for C and Si PKAs. Such a systematic examination of E_d is expected to yield a clear picture of the displacement energy surface. Moreover, E_d has been determined by computer simulation for the first time in several directions for 6H–SiC in an effort to compare the displacement energy surfaces of the two most commonly studied polytypes. In addition, the production of defects in low-energy displacement cascades has been examined by simulating 30 different 500 eV cascades involving both Si and C PKAs along five different directions in 3C–SiC. Most MD studies on displacement cascades have focussed on the structure of individual cascades, without much emphasis on the statistics of the defect production process. The present work addresses this need and facilitates the interpretation of previous experimental studies of defect production in SiC.

Table 1
Structures of 3C–SiC and 6H–SiC

Structure property	3C	6H
Spacegroup	$F\bar{4}3m$	$P6_3mc$
Pearson symbol	CF8	hP12
a (nm)	0.436	0.308
c (nm)		1.512
Equivalent planes	(1 1 1)	(0 0 0 1)

Table 2
Experimentally determined displacement energies (E_d) in SiC

E_d (eV)	Polytype	Sublattice	Direction	Technique	Ref.
22	6H	C	Average	MCL[a]	[5]
30–35	6H	Si	Average	RBS/C	[4]
97	6H	Si	[0 0 0 1]	TEM	[6]
54[b]	3C	C	[1 1 0]	TEM	[7]
54[b]	3C	C	[1 0 0]	TEM	[7]
90[b]	3C	C	[1 1 1]	TEM	[7]
106	3C	Si	[1 1 1]	TEM	[8]

[a] Minority carrier lifetime.
[b] Zinkle and Kinoshita [9] have suggested that these observations correspond to the Si sublattice with E_d values of 45, 45 and 77 eV, respectively.

Table 3
Summary of calculated displacement energies (E_d) in 3C–SiC

Potential	[1 0 0]		[1 1 0]		[1 1 1]		$[\bar{1}\,\bar{1}\,\bar{1}]$		Ref.
	C	Si	C	Si	C	Si	C	Si	
Pearson	13	40	15	146	10	53	20	158	[10]
Tersoff[a]	40	35	30	85	25	35	50	40	[11]
Tersoff[b]	14	43	18	66	22			47	[12]
Tersoff[c] (This work)	31	36	38	71	28	113	71	39	[13]
First principles	29		39		28				[15]

[a] Earlier version of the Tersoff potential [17].
[b] Ziegler–Biersack–Littmark potential used for short-range interactions.
[c] Optimized version of Tersoff potential with ab initio repulsive potential.

2. Details of the simulation

Molecular dynamics simulations were performed using the MOLDYCASK [22] code modified to run on a desktop workstation at Pacific Northwest National Laboratory. An isothermal isobaric (NPT) ensemble [23] was used to heat 3C–SiC at temperatures up to 6000 K in an effort to evaluate the potential by simulating the decomposition of SiC. In this simulation, the MD cell contained 998 atoms ($5\times5\times5$ unit cells with a C and a Si vacancy). The structure of the system was analyzed using global and partial radial distribution functions (RDF). The displacement energy calculations and cascade simulations, however, were performed in the microcanonical ensemble (NVE) with constant number of atoms, volume, and energy (NVE). For 3C–SiC, the simulation cell consisted of 8000 atoms ($10\times10\times10$ unit cells), while the cell for the 6H–SiC contained 1344 atoms. Periodic boundary conditions were employed, and care was taken to ensure that the PKA did not channel through the cell. The simulations were performed at 300 K, because experimental studies have shown that reproducible values of E_d are obtained at this temperature [7].

The interactions between the atoms were modeled using the most recent parameters of the Tersoff potential [18,19]. The cutoff distances were scaled with the cell volume to avoid unphysical effects [24]. The Tersoff potential was joined smoothly to a realistic repulsive potential [21] instead of the more commonly used but less realistic Ziegler–Biersack–Littmark (ZBL) potential [25]. The functional form of the potential and the parameters used have been discussed in detail elsewhere [13]. The simulation cell was initially held at 300 K for 20 ps, which was much longer than the time (about 0.2 ps) needed for the system to attain equilibrium. An atom near the center of the cell was then given a kinetic energy ranging from 10 to 500 eV along a chosen direction, and the atoms were allowed to relax for time periods up to 10 ps. Along each direction, the simulation was repeated for different PKA energies and on both sublattices until a stable Frenkel pair was produced. The intermediate configurations were periodically saved to enable the calculation of the number and type of defects produced.

3. Results and discussion

3.1. Phase stability

Fig. 1 shows the potential energy per atom in 3C–SiC as a function of temperature over the range from 300 to 6000 K. The abrupt increase in energy between 4800 and 4900 K indicates the occurrence of a phase transformation. The energy increases smoothly with temperature for the 10 data points below and the 7 data points above the transformation. The phase diagram [26] shows that 3C–SiC does not melt when heated, but instead decomposes by a peritectic transformation at about 2820 K into solid C and a liquid of 27 at.% C. The interatomic potentials used in the present work overes-

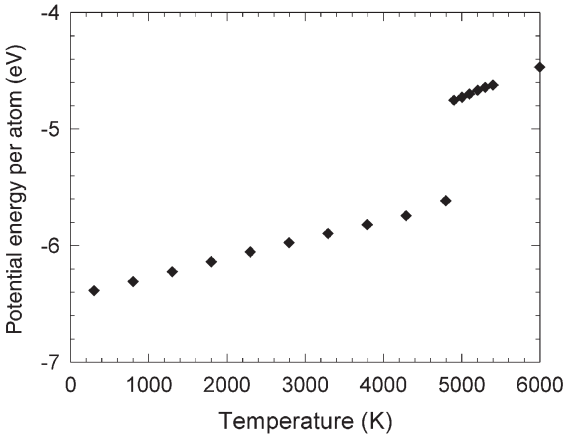

Fig. 1. Potential energy per atom of 3C–SiC as a function of temperature.

timate this transformation temperature. A previous MD simulation [11] had determined the melting temperature of SiC to be about 2800 K, but had not discussed the structural and bonding characteristics of the resulting liquid. Such information is needed to determine if the simulation cell undergoes melting or a peritectic transformation. The differences between the present study and the previous work [11] may arise from differences in the parameters of the Tersoff potential, the nature of the short-range repulsive potential, and our use of the more realistic NPT instead of NVE ensemble.

The structure of the simulation cell above and below the transformation temperature was examined using RDF. Fig. 2 shows the global RDF, $g(r)$, for the 3C–SiC simulation cell. At 4800 K, $g(r)$ is characteristic of a crystalline solid, while at 4900 K a liquid with high atomic mobility is observed. The differences are clearly evident when the g_{Si-Si} and g_{C-C} partial RDFs are examined. The g_{C-C} curve is shown in Fig. 3 to illustrate this point. At 4800 K, g_{C-C} is characteristic of 3C–SiC with considerable peak broadening and the appearance of a small peak around 0.15 nm. However, at 4900 K, g_{C-C} exhibits an intense first peak at 0.153 nm, which is the nearest neighbor distance in diamond (as compared to 0.142 nm in graphite). At and above 4900 K, the structure consists of C clusters linked by C–Si bonds to a Si–Si network. At 4900 K, the first minimum in the RDF occurs at about 0.20 and 0.24 nm, respectively, for g_{C-C} and g_{Si-C}. Based on these cut-off distances, the average C atom has about 1.5 C neighbors and 2.45 Si neighbors at 4900 K. The corresponding numbers at 4800 K are 0.06 and 3.93, respectively, indicating that chemical order is preserved up to the transformation temperature. The structural and bonding characteristics of SiC above 4800 K are similar to those reported for amorphous SiC based on an ab initio molecular dynamics simulation [27].

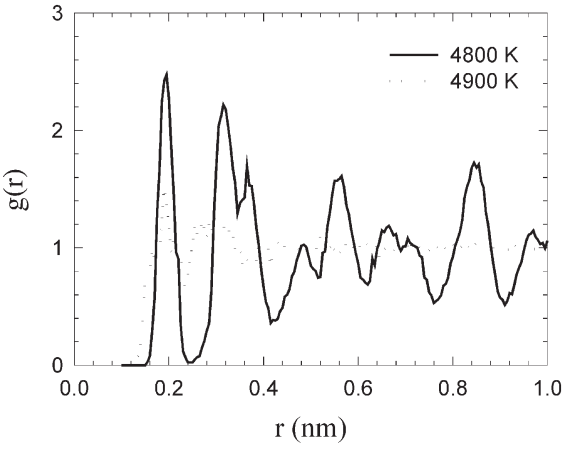

Fig. 2. Global radial distribution function of 3C–SiC at 4800 and 4900 K.

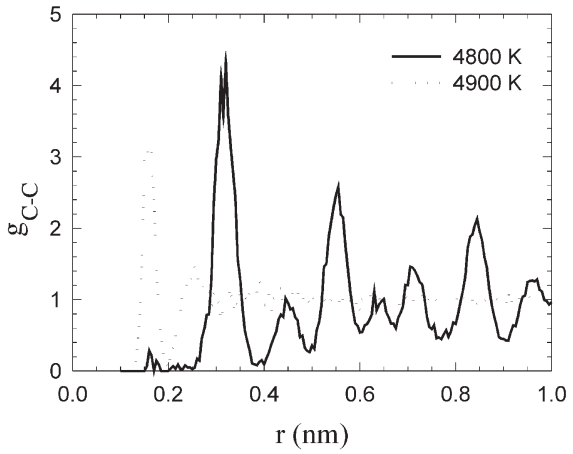

Fig. 3. Partial C–C radial distribution function of 3C–SiC at 4800 and 4900 K.

3.2. Displacement energies

Table 4 shows the values of E_d determined for the C and Si sublattices along 26 different directions. The threshold displacement energy is determined by giving a C or Si atom a certain kinetic energy and, depending on the displacement of the atom from its site, repeating the simulation for a higher or lower PKA energy [13]. The margin of uncertainty in E_d is taken as one half of the energy increment used. Two simulations each are run at the lower and upper bounds of E_d to determine that stable displacements are not produced below E_d and that the displacements above E_d are stable. The displaced atom generally reaches its final configuration within 0.25 ps, and the energy of the simulation cell stabilizes within 0.5 ps after PKA introduction. Along some directions, stable Frenkel pairs on the non-PKA sublattice are produced at energies below that necessary for permanent displacements on the PKA sublattice. Nonetheless, the PKA atom is considered permanently displaced only if a stable Frenkel pair remains on the PKA sublattice at 2 ps following PKA introduction. For instance, a 65 eV Si PKA along [1 1 1] can produce a stable C Frenkel pair because of the low E_d (28 eV) for C along [1 1 1]; however, a Si PKA with an energy of 113 eV is required to create a stable displacement on the Si sublattice. Thus, a Si PKA along [1 1 1] with energy between 65 and 112 eV will not itself be permanently displaced but will produce one or more C Frenkel pairs. The implications of this behavior will be discussed below.

The margin of uncertainty in E_d is ±1 eV for the [0 0 1], [0 1 1], [0 $\bar{1}$ $\bar{1}$], [1 1 1], and [$\bar{1}$ $\bar{1}$ $\bar{1}$] directions and ±5 eV for the higher index directions, because a broader energy interval between successive PKA simulations was used for the latter. As noted previously [13] and indicated in Table 3, the results along several principal

Table 4
Displacement energies (E_d) in 3C–SiC determined in the present work

Direction	C (eV)	Si (eV)
[0 0 1]	31	36
[0 1 1 0]	33	38
[0 1 5]	33	42
[0 3 1 0]	45	48
[0 2 5]	50	77
[0 1 2]	55	71
[0 3 5]	37	83
[0 7 10]	28	95
[0 4 5]	26	83
[0 9 10]	26	71
[0 1 1]	38	71
[1 8 8]	34	85
[1 4 4]	36	111
[1 3 3]	24	107
[1 2 2]	32	115
[2 3 3]	21	135
[5 6 6]	21	135
[1 1 1]	28	113
[0 $\bar{1}$ $\bar{1}$]	38	71
[$\bar{1}$ $\bar{8}$ $\bar{8}$]	40	68
[$\bar{1}$ $\bar{4}$ $\bar{4}$]	36	45
[$\bar{1}$ $\bar{3}$ $\bar{3}$]	34	45
[$\bar{1}$ $\bar{2}$ $\bar{2}$]	42	40
[$\bar{2}$ $\bar{3}$ $\bar{3}$]	60	39
[$\bar{5}$ $\bar{6}$ $\bar{6}$]	44	46
[$\bar{1}$ $\bar{1}$ $\bar{1}$]	71	39

directions are in excellent agreement with accurate ab initio calculations [15].

Fig. 4 shows the PKA displacement distance and potential energy per atom as a function of time elapsed after PKA introduction for 23 and 25 eV C PKA along [0 0 0 1] in 6H–SiC. For the 23 eV case, the PKA returns to its original position after exploring a series of unstable configurations, and its potential energy decreases to its original value. On the other hand, the 25 eV C PKA results in a stable C Frenkel pair separated by about 0.34 nm. From this result, the E_d for C along [0 0 0 1] in 6H–SiC is estimated to be 24 ± 1 eV. The system relaxes to its final configuration within 0.5 ps after PKA introduction, and the kinetic energy of the PKA is lost mostly as heat. The dissipation of heat generally resulted in a temperature rise of less than 100 K for 3C–SiC and 200 K for 6H–SiC. The larger temperature increase for 6H–SiC is a consequence of the use of a smaller simulation cell. Table 5 lists E_d for Si and C PKAs along several low-index directions. These results, to the best of our knowledge, represent the first MD calculation of displacement energies in 6H–SiC.

The displacement energy surface shows many similarities in the two polytypes studied. First, the displacement energy surface is highly anisotropic. In 3C–SiC, the values of E_d for C range from 21 eV along [2 3 3]

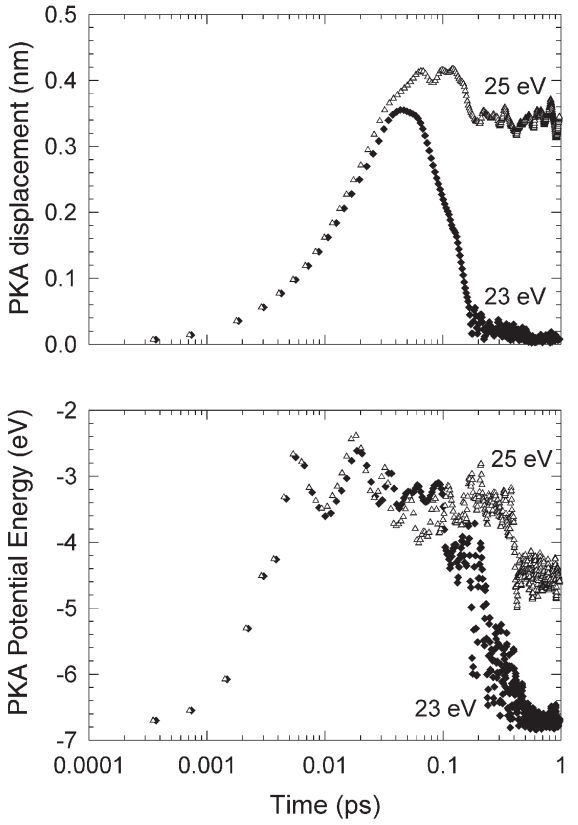

Fig. 4. PKA displacement and potential energy for 23 and 25 eV C PKA along [0 0 0 1] in 6H–SiC. E_d is 24 ± 1 eV.

to 71 eV along [$\bar{1}$ $\bar{1}$ $\bar{1}$], and E_d for Si varies from 36 eV along [0 0 1] to 135 eV along [2 3 3]. In 6H–SiC, E_d for C ranges from 24 eV along [1 $\bar{1}$ 0 0] to 65 eV along [0 0 0 $\bar{1}$], and E_d for Si varies from 35 eV along [0 0 0 $\bar{1}$] to 120 eV along [0 0 0 1]. Second, the minimum E_d values for the 2 polytypes are similar, about 21 eV for C and 35 eV for Si. Third, E_d is comparable for the equivalent directions, [1 1 1] and [0 0 0 1] or [$\bar{1}$ $\bar{1}$ $\bar{1}$] and [0 0 0 $\bar{1}$], in 3C–SiC and 6H–SiC, respectively, as shown in Table 6. For these directions, E_d changes significantly with a 180° rotation because of the asymmetry in atomic arrangement. For instance, along [1 1 1] in 3C–SiC, a Si atom has a C

Table 5
Displacement energies (E_d) in 6H–SiC calculated in the present work

Direction	C (eV)	Si (eV)
[0 0 0 1]	31 ± 1	120 ± 1
[0 0 0 $\bar{1}$]	65 ± 1	35 ± 1
[0 1 $\bar{1}$ 0] [0 $\bar{1}$ 1 0]	27 ± 1	72 ± 1
[1 0 $\bar{1}$ 0] [$\bar{1}$ 0 1 0]	27 ± 1	71 ± 1
[1 1 $\bar{2}$ 0] [$\bar{1}$ $\bar{1}$ 2 0]	26 ± 1	76 ± 1
[1 $\bar{1}$ 0 0] [$\bar{1}$ 1 0 0]	24 ± 1	76 ± 1

Table 6
Comparison of displacement energies along equivalent directions in 3C–SiC and 6H–SiC

PKA	Direction	Polytype	E_d (eV)
Si	[1 1 1]	3C	113 ± 1
Si	[0 0 0 1]	6H	120 ± 1
C	[1 1 1]	3C	28 ± 1
C	[0 0 0 1]	6H	31 ± 1
Si	$[\bar{1}\,\bar{1}\,\bar{1}]$	3C	39 ± 1
Si	$[0\,0\,0\,\bar{1}]$	6H	35 ± 1
C	$[\bar{1}\,\bar{1}\,\bar{1}]$	3C	71 ± 1
C	$[0\,0\,0\,\bar{1}]$	6H	65 ± 1

nearest neighbor at a distance of 0.189 nm, while in the opposite direction there is no such nearest neighbor for a distance of 0.566 nm and vice versa for a C atom.

The interstitials produced in these low energy (less than 135 eV) displacement events are mostly dumb-bell configurations. Fig. 5 shows a Si dumb-bell interstitial (shown in black) produced by a [0 0 1] Si PKA within a section of the SiC simulation cell. The Si vacancy that is produced is at the face-center position of the bottom face. The Si dumb-bell interstitial has coordinates (in units of lattice parameter) for the two Si ions of (0.0, 0.0, 0.75) and (−0.04, 0.03, 1.2) with respect to the vacancy. Two neighboring C ions are displaced from (−0.25, 0.25, 0.75) and (0.25, −0.25, 0.75) to about (−0.3, 0.3, 0.66) and (0.3, −0.3, 0.66), respectively. The average energy of formation for the dumb-bell is 2.8 eV/atom (2.5 eV from each interstitial in the dumb-bell and 0.3 eV each from the distorted C atoms). In the case of a C PKA along [0 0 1] resulting in a vacancy at coordinates (0.25, 0.25, 0.25), a dumb-bell interstitial is formed with C coordinates at (0.4, 0.22, 1.21) and (0.06, 0.26, 1.21) about the (0.25, 0.25, 1.25) C lattice site. Since the C atoms are smaller than the Si atoms, the C dumb-bell is accommodated without significant strain on the neighboring Si atoms. The average energy of formation of the C dumb-bell is 2.2 eV/atom. Isolated Si or C interstitials and other defects are also produced along certain directions. For instance, a 121 eV Si PKA along [0 0 0 1] in 6H–SiC results in a Si interstitial, a C interstitial, a Si anti-site, and a C anti-site defect, which indicates that four permanent defects are produced at the E_d for Si along [0 0 0 1].

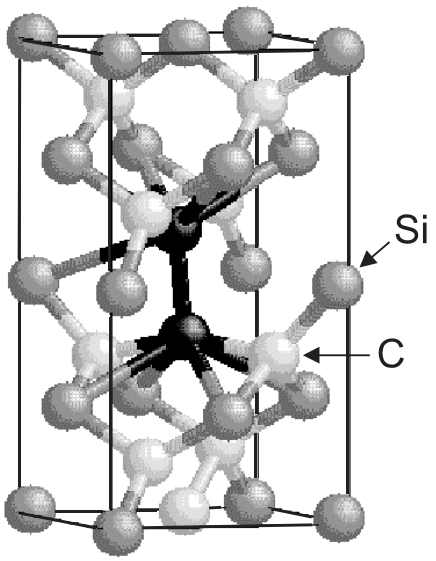

Fig. 5. Si dumb-bell interstitial (black) produced by a 50 eV Si PKA along [0 0 1] (upward direction) in 3C–SiC.

The present work represents the most comprehensive simulation study of displacement energies in SiC. The minimum threshold displacement energies in SiC (Tables 4 and 5) are 21 eV for C and 35 eV for Si, which are in good agreement with the values of 20 and 40 eV for C and Si, respectively, recommended by Zinkle and Kinoshita [9]. The geometric average values of E_d over all the crystallographic directions considered in this study are calculated by taking into account the multiplicity of each direction (i.e., number of equivalent directions). These averages are 37 and 73 eV for C and Si, respectively, in 3C–SiC and 31 eV for C and 75 eV for Si in 6H–SiC. These values are considerably higher than the values recommended by Zinkle and Kinoshita [9]. The difference is due to the anisotropy of the E_d surface, which leads to excessive contributions to the average from directions with high E_d values. However, along many of these high E_d directions, subthreshold recoil energies on one sublattice can lead to displacement events on the other sublattice. In the case of Si displacements along [1 1 1] that was discussed above, a Si PKA (or recoil) along [1 1 1] with energy between 65 and 112 eV will not itself be permanently displaced but will produce one or more C Frenkel pairs due to the low E_d for C along this direction. This behavior represents a potential problem for Monte Carlo calculations of displacement damage, such as in TRIM [25], that use the threshold displacement energy for each species as the cutoff energy for further displacements in the calculations. Thus, if 113 eV is used as E_d for Si along [1 1 1], then the number of displacements would be underestimated because C atoms displaced by subthreshold Si recoils, with energies between 65 and 112 eV, would not be included. This suggests that the effective displacement energies will be lower than the geometric average values calculated in the present study.

3.3. Low-energy cascades

In a collision cascade, Frenkel pairs should form preferentially along directions with low E_d. In order to investigate this hypothesis regarding defect production in cascades, 15 separate cascades have been investigated for both 500 keV Si and 500 keV C PKAs in 3C–SiC. This study involved 3 Si PKAs and 3 C PKAs along each of five low-index directions in 3C–SiC (namely, [0 0 1], [0 0 $\bar{1}$], [1 1 0], [1 1 1], and [$\bar{1}\,\bar{1}\,\bar{1}$]), including several high E_d directions. The 15 C PKAs produced an average of about 9.0 displacements, as shown in Fig. 6, while the 15 Si PKAs generated about 9.75 displacements, as shown in Fig. 7. In these low energy cascades, C and Si interstitials, replacements and a few anti-site defects are produced. Further details of these cascades will be included in a forthcoming article on displacement cascades in SiC. The C displacements outnumbered the Si displacements by a factor of about 2 for the Si PKAs and a factor of about 4 for the C PKAs.

One can calculate the average E_d value for these simulations using the modified Kinchin–Pease model [28],

$$E_d = \frac{0.4E_{PKA}}{N_{disp}}. \quad (1)$$

Here, E_{PKA} is the PKA energy in the MD simulation (500 eV) and N_{disp} the number of displacements produced. E_{PKA} is also known as damage energy in the Lindhard–Sharff–Schiøtt (LSS) theory [29]. It represents the kinetic energy portion of the recoil energy and excludes the energy lost in electronic excitations, which is not taken into account in the present MD simulations. TRIM calculations [25] show that the electronic energy loss for a damage energy of about 500 eV in SiC ranges from about 15% for Si recoils to about 29% for C recoils.

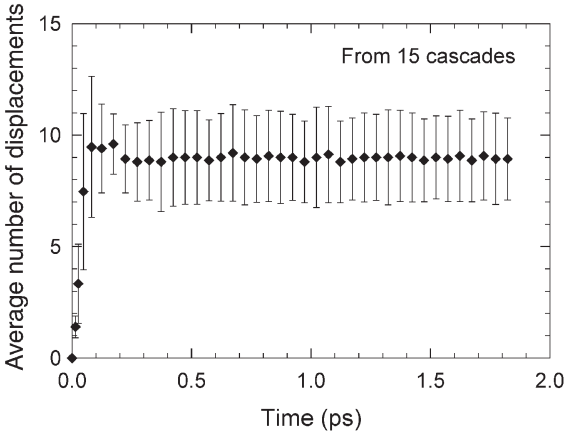

Fig. 6. The number of displacements produced by 500 eV C PKA in 3C–SiC.

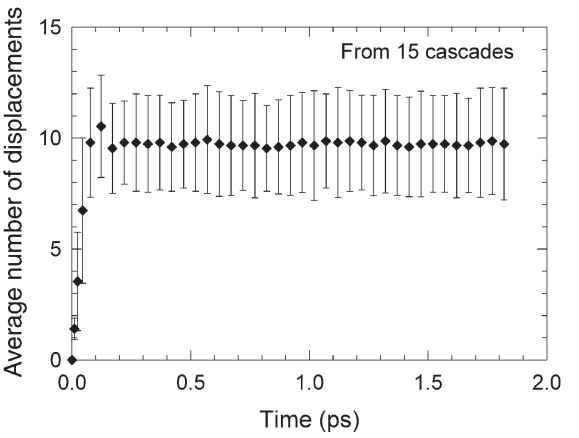

Fig. 7. The number of displacements produced by 500 eV Si PKA in 3C–SiC.

Thus, the damage energy of 500 eV corresponds to approximately a 600 eV Si recoil or a 700 eV C recoil. The displacement energy in SiC averaged over both sublattices, based on Eq. (1), is about 20–22 eV. Weighting the minimum E_d of the 2 sublattices (21 and 35 eV) by the fraction of displacements produced in these cascades, yields 23–26 eV for E_d, in agreement with the above Kinchin–Pease calculation and experimental data [9]. These results indicate that average displacement energies determined, as above, from realistic low-energy cascade simulations offer more reasonable values for E_d than geometric averages over all directions. Furthermore, the results are consistent with the hypothesis that preferential displacement of atoms occurs along low E_d directions, even for PKAs or recoils along high E_d directions. Nonetheless, the simulation along individual directions provides information about the anisotropy of the threshold energy surface and the minimum values for E_d.

4. Conclusions

Using MD simulations with realistic potentials, the present study has demonstrated the phase separation of 3C–SiC upon heating and determined the threshold displacement energies in both 3C–SiC and 6H–SiC along a range of directions. The simulations show that the displacement energy surfaces in these two polytypes are similar and highly anisotropic. Furthermore, most displacement events result in the formation of dumb-bell interstitials, although some anti-site defects are also observed. These results provide insights into the large scatter in the threshold displacement energy values estimated for SiC from experiments. The E_d values determined along discrete directions by electron

microscopy shows considerable scatter because the displacement energy varies significantly with crystallographic orientation. The electron microscopy technique tends to overestimate E_d because the defects must generally migrate and cluster to be observed. Other techniques determine minimum or average E_d values, and it is difficult to compare E_d values obtained by different techniques. Methods, such as RBS/C, following light-ion irradiation tend to underestimate E_d because amorphization may be produced in addition to isolated defects.

The systematic computer simulations of displacement events in the present work complement previous experimental observations [4–9] and indicate that the minimum E_d values are about 21 and 35 eV for C and Si, respectively, in both 3C–SiC and 6H–SiC. The geometric average E_d values (e.g., 37 eV for C and 73 eV for Si in 3C–SiC) are heavily weighted by large E_d values along directions where subthreshold recoil energies on one sublattice can lead to displacement events on the other sublattice. This suggests that the effective displacement energies should be lower than the geometric average values, which is consistent with the results from the simulation of low-energy cascades. The systematic evaluation of 30 low-energy (500 eV) cascade simulations in 3C–SiC along five different low-index directions indicates that the total defect production is consistent with calculations based on the minimum values of E_d, even for PKAs along high E_d directions; this suggests the preferential displacement of atoms along low E_d directions. Therefore, the minimum E_d values of 21 and 35 eV for C and Si, respectively, should be considered for use in calculations of defect production in SiC.

Acknowledgements

This work was supported by the Division of Materials Science, Office of Basic Energy Sciences, US Department of Energy under Contract DE-AC06-76RLO 1830 and was performed at Pacific Northwest National Laboratory. R.D. thanks the Associated Western Universities for a Faculty Fellowship.

References

[1] R.H. Jones, L.L. Snead, A. Kohyama, P. Fenici, Fusion Eng. Des. 41 (1998) 15.
[2] W. Wesch, Nucl. Instrum. and Meth. B 116 (1996) 305.
[3] W.J. Choyke, G. Pensl, MRS Bull. 22 (3) (1997) 25.
[4] W. Jiang, W.J. Weber, S. Thevuthasan, D.E. McCready, Nucl. Instrum. and Meth. B 148 (1999) 557.
[5] A.L. Barry, B. Lehmann, D. Fritsch, D. Braunig, IEEE Trans. Nuc. Sci. 38 (1991) 1111.
[6] H. Inui, H. Mori, H. Fujita, Philos. Mag. B 61 (1990) 107.
[7] I.A. Hønstvet, R.E. Smallman, P.M. Marquis, Philos. Mag. A 41 (1980) 201.
[8] B. Hudson, A.E. Sheldon, J. Microsc. 97 (1973) 113.
[9] S.J. Zinkle, C. Kinoshita, J. Nucl. Mater. 251 (1997) 200.
[10] A. El-Azab, N.M. Ghoniem, J. Nucl. Mater. 191/194 (1992) 1110.
[11] J. Wong, T. Diaz de la Rubia, M.W. Guinan, M. Tobin, J.M. Perlado, A.S. Perez, J. Sanz, J. Nucl. Mater. 212–215 (1994) 143.
[12] H. Hensel, H.M. Urbassek, Nucl. Instrum. and Meth. B 142 (1998) 287.
[13] R. Devanathan, T. Diaz de la Rubia, W.J. Weber, J. Nucl. Mater. 253 (1998) 47.
[14] J.M. Perlado, L. Malerba, T. Diaz de la Rubia, in: S.J. Zinkle, G. Lucas, R. Ewing, J. Williams (Eds.), Microstructural Processes in Irradiated Materials, MRS Symposia Proceedings No. 540, Materials Research Society, Pittsburgh, PA, 1999, p. 171.
[15] W. Windl, T.J. Lenosky, J.D. Kress, A.F. Voter, Nucl. Instrum. and Meth. B 141 (1998) 61.
[16] E. Pearson, T. Takai, T. Halicioglu, W. Tiller, J. Cryst. Growth 70 (1984) 33.
[17] J. Tersoff, Phys. Rev. B 39 (1989) 5566.
[18] J. Tersoff, Phys. Rev. B 49 (1994) 16349.
[19] J. Tersoff, Phys. Rev. Lett. 64 (1990) 1757.
[20] H. Huang, N.M. Ghoniem, J.K. Wong, M.I. Baskes, Modelling Simul. Mater. Sci. Eng. 3 (1995) 615.
[21] K. Nordlund, N. Runeberg, D. Sundholm, Nucl. Instrum. and Meth. B 132 (1997) 45.
[22] T.D. de la Rubia, M.W. Guinan, J. Nucl. Mater. 174 (1990) 151.
[23] H.C. Andersen, J. Chem. Phys. 72 (4) (1980) 2384.
[24] M. Tang, S. Yip, Phys. Rev. B 52 (1994) 15150.
[25] J.F. Ziegler, J.P. Biersack, U. Littmark, The Stopping and Range of Ions in Solids, Pergamon, Oxford, 1985.
[26] R.W. Olesinski, G.J. Abbaschian, Bull. Alloy Phase Diag. 5 (5) (1984) 486.
[27] F. Finocchi, G. Galli, M. Parrinello, C. Bertoni, Phys. Rev. Lett. 68 (20) (1992) 3044.
[28] M.J. Norgett, M.T. Robinson, I.M. Torrens, Nucl. Eng. Des. 33 (1975) 50.
[29] M.T. Robinson, J. Nucl. Mater. 216 (1994) 1.